Research Article Vol. 2, No. 3 / 15 March 2019 / OSA Continuum 874

Enhanced stability and sensitivity of slope-assisted Brillouin optical correlation-domain reflectometry using polarization-maintaining fibers

HEEYOUNG LEE,* YOSUKE MIZUNO, AND KENTARO NAKAMURA

Institute of Innovative Research, Tokyo Institute of Technology, 4259, Nagatsuta-cho, Midori-ku, Yokohama 226-8503, Japan
*hylee@sonic.pi.titech.ac.jp

Abstract: We show that, even when a polarization scrambler is switched off, PMF-based SA-BOCDR can operate with higher stability than that of standard silica-fiber-based systems. This leads to reduced cost and enables the use of the optimized state of polarization for higher sensitivity. After investigation of the strain/temperature dependencies of the Brillouin frequency shift and the Brillouin spectral power in the PMF, we show that the strain/temperature sensitivity of the PMF-based SA-BOCDR is 1.4 times the value of the standard silica-fiber-based configuration; we then demonstrate distributed temperature measurement with higher stability and sensitivity.

1. Introduction

Distributed strain and temperature sensing is a key technology for monitoring a variety of civil infrastructures and enhancing human safety. In particular, fiber-optic distributed sensing techniques based on Brillouin scattering [1] are immensely promising for their ability to detect sub-centimeter or even sub-millimeter strained or heated sections along long optical fibers [2,3]. From the aspect of light injection to sensing fibers, Brillouin sensors can be categorized into two-end-access "analysis" and single-end-access "reflectometry". The former includes Brillouin optical time-, frequency-, and correlation-domain analysis (BOTDA [4–6], BOFDA [7–9], and BOCDA [10–14]), while the latter includes Brillouin optical time-, frequency-, and correlation-domain reflectometry (BOTDR [15–17], BOFDR [18], and BOCDR [19–26]). Although analysis systems generally have higher signal-to-noise ratios (SNRs) owing to the use of stimulated Brillouin scattering, reflectometers based on spontaneous Brillouin scattering have higher degrees of freedom in embedding the sensing fibers into structures and thus are convenient for end-users. Here, we focus on BOCDR, which is the only scheme that can simultaneously achieve single-end accessibility, high spatial resolution, and cost efficiency.

Since its first proposal [19], BOCDR has been vigorously studied, and many configurations have been developed to improve its performance [21–26]. Recently, two types of high-speed BOCDR systems have been implemented. One is phase-detected (PD-) BOCDR [26], which enables a >100 kHz sampling rate, but the strain dynamic range is severely limited. The other is slope-assisted (SA-) BOCDR [27], which exploits not the Brillouin frequency shift (BFS) itself but the power on the slope of the Brillouin gain spectrum (BGS). The sampling rate of SA-BOCDR is lower than that of PD-BOCDR, but SA-BOCDR has a wider strain dynamic range. In addition, SA-BOCDR has been shown to possess a unique "beyond-nominal-resolution" effect [28], with which a 2-mm strained section has been detected (sub-millimeter detection has also theoretically shown to be feasible) [3]. In addition, very recently, an example of SA-BOCDR-based composite structural diagnosis has been reported, showing its practical use in

#357479 https://doi.org/10.1364/OSAC.2.000874
Journal © 2019 Received 11 Jan 2019; revised 8 Feb 2019; accepted 12 Feb 2019; published 13 Mar 2019

OSA CONTINUUM

the future [29]. Thus, there has been considerable progress on the SA-BOCDR technology, but one of its major drawbacks is the significant polarization-dependent power fluctuations, which lead to unstable operation of the system. To date, to mitigate this noise, a polarization scrambler (PSCR) has been employed in the system [3,27–29], but the averaged state of polarization (SOP) leads to non-ideal sensitivity (as experimentally shown below), and in addition, the use of the PSCR increases the cost and encumbers the downsizing of the system. Polarization diversity has also been employed in BOCDR [30], but the negative situation cannot be remedied because of the use of a polarization switch, and what is worse, the sampling rate inevitably becomes less than half for data processing.

In this paper, to resolve these shortcomings, we develop polarization-scrambling-free SA-BOCDR using a polarization-maintaining fiber (PMF) as a fiber under test (FUT). A PSCR is not employed in this configuration, leading to the cost reduction (when the FUT is relatively short). In addition, what is more important, the SOP can be optimized so that the sensitivity can be higher. First, we experimentally show that, unlike the case where the FUT is a silica single-mode fiber (SMF), PMF-based SA-BOCDR can operate correctly even when the PSCR is switched off. Subsequently, we characterize the fundamental sensing properties, such as the strain/temperature dependencies of the BFS and the Brillouin spectral power in the PMF, and show that the strain sensitivity of the PMF-based SA-BOCDR is 1.4 times higher than that of the conventional configuration. Finally, we demonstrate distributed temperature sensing with higher stability and sensitivity.

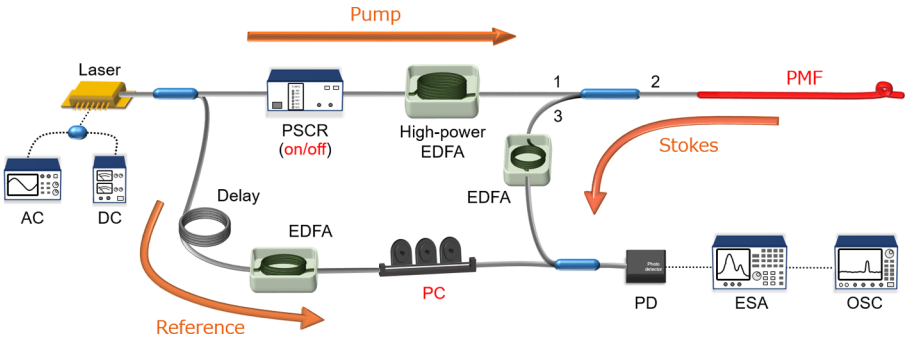

Fig. 1. Experimental setup of SA-BOCDR, in which the polarization scrambler (PSCR) can be switched on and off. EDFA, erbium-doped fiber amplifier; ESA, electrical spectrum analyzer; OSC, oscilloscope; PC, polarization controller; PD, photodetector; PMF, polarization-maintaining fiber.

2. Experimental setup

As the FUTs for distributed measurements, we used a silica SMF (LPSGK-S-SM, Sigma Koki) and a polarization-maintaining and absorption-reducing (PANDA) fiber (most commonly used PMF; P3-1550PM-FC, Thorlabs) [31]. The PANDA fiber had a core diameter of 8.5 μm and a relatively low propagation loss of ~0.4 dB/km. The BFSs of the silica SMF and PANDA fiber were 10.855 and 10.863 GHz, respectively, at 1.55 μm at room temperature (20 °C). The lengths of the two FUTs were both 9.15 m. Figure 1 schematically shows the experimental setup of SA-BOCDR, in which a PSCR can be switched on and off. Compared to the previous report [27], a polarization controller (PC) was newly employed to control the SOP when the PSCR was switched off. The 1.55-μm light from a distributed-feedback laser diode (NLK1C5GAAA, NTT Electronics) was divided into two: pump and reference lights. After amplified to 26 dBm using a high-power erbium-doped fiber amplifier (EDFA), the pump light was injected into the

OSA CONTINUUM

FUT. In this measurement, no special attempt was made to align the polarization state of the pump light to one of the eigenaxes of the PMF. To suppress the Fresnel reflection, a bending loss was applied near the distal end of the FUT. The backscattered Brillouin Stokes light from the FUT was amplified to ~1 dBm using another EDFA and coupled with the reference light. The reference light was amplified to ~2 dBm in advance after passing through a delay fiber (which was employed to avoid the appearance of the zero-optical-path-difference point, i.e., the 0th correlation peak, in the FUT; the length can be shortened to <<1 km, if necessary). Then, using a photodetector (PD), the self-heterodyned optical signal was converted into an electrical signal, which was observed as a BGS using an electrical spectrum analyzer (ESA). The spectral power change at a fixed frequency (10.86 GHz for the PMF (see below) and 10.85 GHz for the SMF) [27] was obtained using a zero-span mode of the ESA and observed using an oscilloscope (OSC) with 256 times averaging. The resolution and video bandwidths of the ESA were 10 MHz and 10 kHz, respectively. The room temperature was 20 °C.

By sinusoidally modulating the optical frequency of the laser output, a correlation peak was generated and scanned along the FUT, which enabled distributed measurement. Based on Eqs. (15) and (16) in [20], the spatial resolution and the measurement range were ~72.5 mm and ~11.4 m by setting the modulation frequency and amplitude to 8.990–9.036 MHz and 1.5 GHz, respectively. Only when we performed single-point measurements to investigate the system performance, the modulation frequency was maintained at 9.023 MHz to obtain the Brillouin signal only from the correlation peak (located 7.15 m away from the end of the second-port pigtail of an optical circulator).

3. Experimental results

First, we performed distributed measurements of Brillouin spectral powers using the partially strained SMF and PMF under three SOPs: 1) optimized using the PC so that the power change at the strained section was maximized, 2) scrambled by switching the PSCR on so that the polarization-dependent power change along the FUTs was suppressed, and 3) anti-optimized using the PC so that the power change at the strained section was minimized. Strains of 1000 $\mu\epsilon$ were applied to 0.3-m-long sections (7.0–7.3 m away from the circulator) in both the FUTs. Figure 2(a) and (b) show the power distributions along the SMF and PMF, respectively, under three SOPs. In the case of the SMF, only when the SOP was scrambled, the power distribution was relatively flat and the strained section was correctly detected. However, when the SOP was optimized, although the strained section was detected with higher strain sensitivity, the baseline was significantly distorted and the distributed measurement was clearly erroneous. In addition, when the SOP was anti-optimized, not only was the distributed measurement erroneous but also even the signal at the strained section was completely buried under the distorted baseline. Thus, when the SMF was used, polarization scrambling was found to be of paramount necessity for correct distributed measurements. In contrast, in the case of the PMF, regardless of the SOPs, the baselines were relatively flat and the strained sections were correctly detected. The strain sensitivity at the strained section was highest at the optimized SOP and lowest at the anti-optimized SOP (note that, when the SOP was scrambled, the results were almost identical between the SMF and PMF). Thus, when the PMF was used, polarization scrambling was not necessary any longer, leading to the cost reduction of the system (when the FUT length is relatively short; considering the high cost of the FUT, the PMF-based configuration is not suitable for long-distance measurements). Besides, from the viewpoint of strain sensitivity, the SOP should be optimized instead of being scrambled.

In the experiments below, we characterized the fundamental operations of PMF-based SA-BOCDR and, in both experiment and theory, quantitatively evaluated how much the strain sensitivity can be improved by optimizing the SOP. First, we investigated the BFS dependencies on strain and temperature in a 0.57-m-long PMF. Without applying frequency modulation, the

OSA CONTINUUM

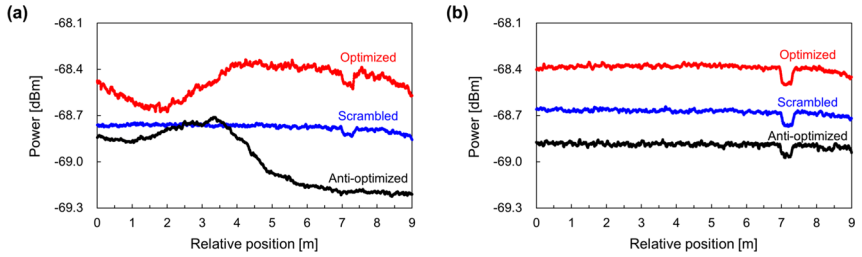

Fig. 2. Spectral power distributions along (a) the SMF and (b) the PMF measured at three different states of polarization, when 1000 μϵ strain was applied to the FUTs (7.0–7.3 m).

BGS was observed when strains from 0 to 4800 μϵ were applied to the whole length of the FUT. The BFS was then plotted as a function of the strain (refer to Appendix). With increasing strain, the BGS linearly shifted to higher frequency with a coefficient of 425 MHz/%, which is ~0.82 times the value in a typical SMF [32]. In the same manner, the BFS dependence on temperature was also measured (refer to Appendix). With increasing temperature from 20 to 80 °C, the BFS also increased with a coefficient of 1.1 MHz/°C, which is almost the same as that in an SMF [33].

Subsequently, after frequency modulation was applied, we measured the BGSs under three different SOPs (Fig. 3(a)). The Brillouin spectral power was highest at the optimized SOP and lowest at the anti-optimized SOP, and using the spectral slope at 10.86 GHz (derived from Fig. 3(a)) and the strain coefficient of the BFS, we can calculate the theoretical strain sensitivities of the spectral power to be 0.96×10^{-4}, 0.76×10^{-4}, and 0.66×10^{-4} dB/με (corresponding to the temperature sensitivities of 2.49×10^{-3}, 1.97×10^{-3}, and 1.72×10^{-3} dB/°C) at optimized, scrambled, and anti-optimized SOPs, respectively. Finally, at three different SOPs, we measured the spectral power dependencies on strain (Fig. 3(b)). The dependencies were almost linear and the coefficients were 1.09×10^{-4}, 0.78×10^{-4}, and 0.69×10^{-4} dB/με at optimized, scrambled, and anti-optimized SOPs, respectively. These values are in moderate agreement with the aforementioned values calculated from the BGS. In this measurement, the standard deviation of the power fluctuations along the non-strained section was approximately +/–0.01 dB, which corresponds to a strain uncertainty of ~190 $\mu\epsilon$. The most important finding here is that the strain sensitivity at the optimized SOP is 1.4 times higher than that at the scrambled SOP. Note that it is difficult to derive this value theoretically based on the theory developed by Deventer *et al.* [34], because the BGS observed in correlation-domain techniques is inherently influenced by bell-shaped background noise [35]. It is also not easy to compare the increased sensitivity with the previously reported sensitivities [3,27–29,36] because SA-BOCDR has the measurement

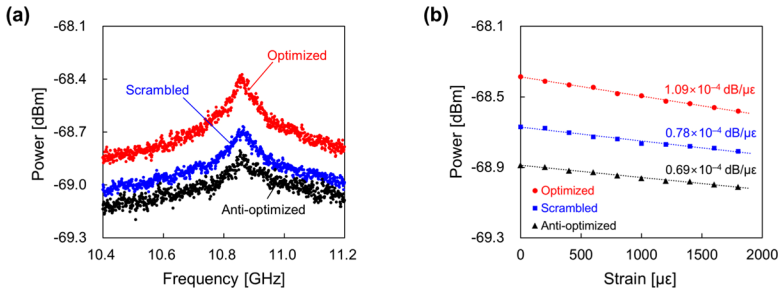

Fig. 3. (a) Measured BGS in the PANDA-type PMF at three different SOPs. (b) Spectral power plotted as a function of the applied strain at three different SOPs. The dotted lines are linear fits.

OSA CONTINUUM

sensitivity dependencies on various experimental conditions including incident light power, spatial resolution, and resolution and video bandwidths of an ESA [36]. Nevertheless, our results clearly indicate that, compared to conventional SMF-based SA-BOCDR, the PMF-based SA-BOCDR can offer polarization-scrambling-free operation with high strain/temperature sensitivity along with the high stability (Refer to Fig. 4(a) (Visualization 1) and Fig. 4(b) (Visualization 2) for demonstrations of distributed temperature measurement using the PMF, in which the spatial resolutions were approximately ~0.2 m and ~0.1 m, respectively).

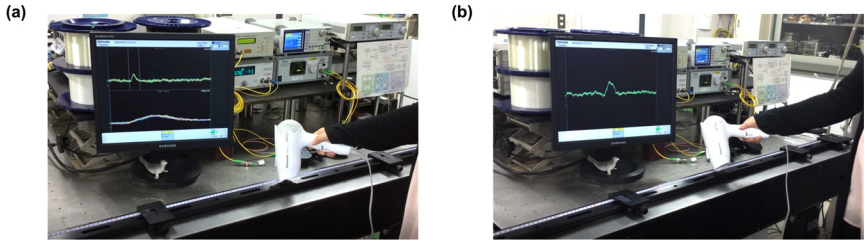

Fig. 4. Demonstration movies of distributed temperature measurement using PMF-based SA-BOCDR. (a) Lower spatial resolution (Visualization 1) and (b) higher spatial resolution (Visualization 2).

4. Conclusions

We developed and characterized the PMF-based SA-BOCDR with no need of polarization scrambling. First, we showed that, unlike silica-SMF-based systems, PMF-based SA-BOCDR can operate with higher stability even when the PSCR is switched off. This enables the use of the optimized SOP for higher sensitivity. After investigation of the strain/temperature dependencies of the BFS and the Brillouin spectral power in the PMF, we finally showed that the strain sensitivity of the PMF-based SA-BOCDR is 1.4 times the value of the standard silica-SMF-based configuration. We also presented two demonstration movies of distributed temperature measurement. Considering the cost of PMFs, this configuration is suitable for high-resolution sensing with a relatively short measurement range. We anticipate that this PMF-based SA-BOCDR will be of significant use for practical structural monitoring in the future owing to its single-end accessibility, higher stability, and enhanced sensitivity.

Appendix

The BFS dependencies on strain and temperature in the PMF are shown in Figs. 5(a) and 5(b), respectively.

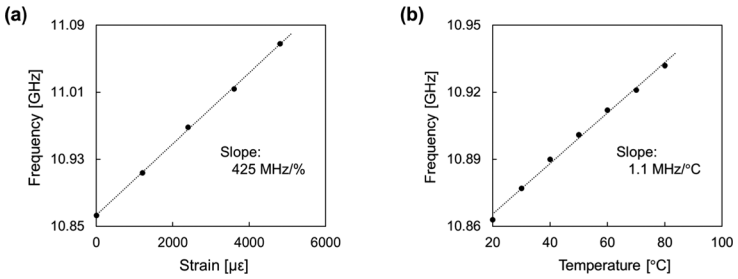

Fig. 5. BFS dependencies on (a) strain and (b) temperature in the PANDA-type PMF. The dotted lines are linear fits.

OSA CONTINUUM

Funding

Japan Society for the Promotion of Science (JSPS) (17H04930, 17J07226); Japan Gas Association; Association for Disaster Prevention Research; Fujikura Foundation; Japan Association for Chemical Innovation (JACI).

References

1. G. P. Agrawal, *Nonlinear Fiber Optics* (Academic Press, 1995).
2. T. D. Vo, J. He, E. Magi, M. J. Collins, A. S. Clark, B. G. Ferguson, C. Xiong, and B. J. Eggleton, "Chalcogenide fiber-based distributed temperature sensor with sub-centimeter spatial resolution and enhanced accuracy," Opt. Express **22**(2), 1560–1568 (2014).
3. H. Lee, Y. Mizuno, and K. Nakamura, "Detection of 2-mm-long strained section in silica fiber using slope-assisted Brillouin optical correlation-domain reflectometry," Jpn. J. Appl. Phys. **57**(2), 020303 (2018).
4. T. Horiguchi and M. Tateda, "BOTDA–nondestructive measurement of single-mode optical fiber attenuation characteristics using Brillouin interaction: theory," J. Lightwave Technol. **7**(8), 1170–1176 (1989).
5. Y. Dong, L. Chen, and X. Bao, "Time-division multiplexing-based BOTDA over 100 km sensing length," Opt. Lett. **36**(2), 277–279 (2011).
6. Y. Peled, A. Motil, L. Yaron, and M. Tur, "Slope-assisted fast distributed sensing in optical fibers with arbitrary Brillouin profile," Opt. Express **19**(21), 19845–19854 (2011).
7. D. Garus, K. Krebber, and F. Schliep, "Distributed sensing technique based on Brillouin optical-fiber frequency-domain analysis," Opt. Lett. **21**(17), 1402–1404 (1996).
8. R. Bernini, A. Minardo, and L. Zeni, "Distributed sensing at centimeter-scale spatial resolution by BOFDA: Measurements and signal processing," IEEE Photon. J. **4**(1), 48–56 (2012).
9. A. Minardo, R. Bernini, and L. Zeni, "Distributed temperature sensing in polymer optical fiber by BOFDA," IEEE Photon. Technol. Lett. **26**(4), 387–390 (2014).
10. K. Hotate and T. Hasegawa, "Measurement of Brillouin gain spectrum distribution along an optical fiber using a correlation-based technique–Proposal, experiment and simulation–," IEICE Trans. Electron. **E83-C**(3), 405–412 (2000).
11. K. Y. Song, M. Kishi, Z. He, and K. Hotate, "High-repetition-rate distributed Brillouin sensor based on optical correlation-domain analysis with differential frequency modulation," Opt. Lett. **36**(11), 2062–2064 (2011).
12. A. López-Gil, S. Martin-Lopez, and M. Gonzalez-Herraez, "Phase-measuring time-gated BOCDA," Opt. Lett. **42**(19), 3924–3927 (2017).
13. C. Zhang, M. Kishi, and K. Hotate, "5,000 points/s high-speed random accessibility for dynamic strain measurement at arbitrary multiple points along a fiber by Brillouin optical correlation domain analysis," Appl. Phys. Express **8**(4), 042501 (2015).
14. W. Zou, C. Jin, and J. Chen, "Distributed strain sensing based on combination of Brillouin gain and loss effects in Brillouin optical correlation domain analysis," Appl. Phys. Express **5**(8), 082503 (2012).
15. T. Kurashima, T. Horiguchi, H. Izumita, S. Furukawa, and Y. Koyamada, "Brillouin optical-fiber time domain reflectometry," IEICE Trans. Commun. **E76-B**(4), 382–390 (1993).
16. A. Masoudi, M. Belal, and T. P. Newson, "Distributed dynamic large strain optical fibre sensor based on the detection of spontaneous Brillouin scattering," Opt. Lett. **38**(17), 3312–3315 (2013).
17. G. Tu, X. Zhang, Y. Zhang, Z. Ying, and L. Lv, "Strain variation measurement with short time Fourier transform-based Brillouin optical time-domain reflectometry sensing system," Electron. Lett. **50**(22), 1624–1626 (2014).
18. A. Minardo, R. Bernini, R. Ruiz-Lombera, J. Mirapeix, J. M. Lopez-Higuera, and L. Zeni, "Proposal of Brillouin optical frequency-domain reflectometry (BOFDR)," Opt. Express **24**(26), 29994–20001 (2016).
19. Y. Mizuno, W. Zou, Z. He, and K. Hotate, "Proposal of Brillouin optical correlation-domain reflectometry (BOCDR)," Opt. Express **16**(16), 12148–12153 (2008).
20. Y. Mizuno, W. Zou, Z. He, and K. Hotate, "Operation of Brillouin optical correlation-domain reflectometry: theoretical analysis and experimental validation," J. Lightwave Technol. **28**(22), 3300–3306 (2010).
21. N. Hayashi, Y. Mizuno, and K. Nakamura, "Distributed Brillouin sensing with centimeter-order spatial resolution in polymer optical fibers," J. Lightwave Technol. **32**(21), 3999–4003 (2014).
22. R. Shimizu, M. Kishi, and K. Hotate, "Enlargement of measurement function in Brillouin optical correlation-domain reflectometry with combining four performance improvement schemes," Proc. SPIE **10323**, 1032390 (2017).
23. Y. Mizuno, N. Hayashi, H. Fukuda, and K. Nakamura, "Single-end-access distributed strain sensing with wide dynamic range using higher-speed Brillouin optical correlation-domain reflectometry," Jpn. J. Appl. Phys. **56**(7), 072501 (2017).
24. Y. Yao, M. Kishi, and K. Hotate, "Brillouin optical correlation domain reflectometry with lock-in detection scheme," Appl. Phys. Express **9**(7), 072501 (2016).
25. N. Hayashi, Y. Mizuno, and K. Nakamura, "Characterization of stimulated Brillouin scattering in polymer optical fibers based on lock-in-free pump-probe technique," J. Lightwave Technol. **31**(19), 3162–3166 (2013).
26. Y. Mizuno, N. Hayashi, H. Fukuda, K. Y. Song, and K. Nakamura, "Ultrahigh-speed distributed Brillouin reflectometry," Light: Sci. Appl. **5**(12), e16184 (2016).

OSA CONTINUUM

27. H. Lee, N. Hayashi, Y. Mizuno, and K. Nakamura, "Slope-assisted Brillouin optical correlation-domain reflectometry: proof of concept," IEEE Photon. J. **8**(3), 1–7 (2016).
28. H. Lee, N. Hayashi, Y. Mizuno, and K. Nakamura, "Operation of slope-assisted Brillouin optical correlation-domain reflectometry: comparison of system output with actual frequency shift distribution," Opt. Express **24**(25), 29190–29197 (2016).
29. H. Lee, Y. Ochi, T. Matsui, Y. Matsumoto, Y. Tanaka, H. Nakamura, Y. Mizuno, and K. Nakamura, "Distributed strain measurement and possible breakage detection of optical-fiber-embedded composite structure using slope-assisted Brillouin optical correlation-domain reflectometry," Appl. Phys. Express **11**(7), 072501 (2018).
30. O. Furukawa, S. Tezuka, M. Tsukamoto, S. Matsuura, M. Kishi, and K. Hotate, "Beyond 21 km distributed strain measurement with Brillouin optical correlation-domain reflectometry using polarization diversity method and temporal gating scheme," IEEJ Trans. Fund. Mater. **137**(1), 52–57 (2017). [In Japanese]
31. Y. Sasaki, K. Okamoto, T. Hosaka, and N. Shibata, "Polarization-maintaining and absorption-reducing fibers," in *Optical Fiber Communication Conference, 1982 OSA Technical Digest Series* (Optical Society of America, 1982), paper ThCC6.
32. T. Horiguchi, T. Kurashima, and M. Tateda, "Tensile strain dependence of Brillouin frequency shift in silica optical fibers," IEEE Photon. Technol. Lett. **1**(5), 107–108 (1989).
33. T. Kurashima, T. Horiguchi, and M. Tateda, "Thermal effects on the Brillouin frequency shift in jacketed optical silica fibers," Appl. Opt. **29**(15), 2219–2222 (1990).
34. M. O. van Deventer and A. J. Boot, "Polarization properties of stimulated Brillouin scattering in single-mode fibers," J. Lightwave Technol. **12**(4), 585–590 (1994).
35. K. Y. Song, Z. He, and K. Hotate, "Optimization of Brillouin optical correlation domain analysis system based on intensity modulation scheme," Opt. Express **14**(10), 4256–4263 (2006).
36. H. Lee, Y. Mizuno, and K. Nakamura, "Measurement sensitivity dependencies on incident power and spatial resolution in slope-assisted Brillouin optical correlation-domain reflectometry," Sens. Actuators A **268**, 68–71 (2017).